

A High-Gain and Beam-Scanning Variable Inclination Continuous Transverse Stub Array Antenna Based on Linear-Gradient Stub at Ku Band

Jie Liu^{1, 2}, Shufu Dong^{1, *}, Qiurong Zheng^{1, *}, Jiayu Yu^{1, 2}, and Fei Xu³

Abstract—A novel Variable Inclination Continuous Transverse Stub (VICTS) antenna element and array model is proposed in this paper. The bandwidth and gain of the element are increased by adopting a linear-gradient stub, matching structure, and rectangular grating slow-wave structure (SWS). A circular array can be obtained by arranging antenna units of different lengths linearly. The array antenna uses a bow-parabolic box antenna as the line source generator (LSG) and utilizes a double-layer transition waveguide structure to realize the propagation of planar wave. Finally, a wide range of beam scanning in the elevation plane was achieved. The results of the simulation and antenna prototype test are in good agreement. Showing the impedance matching characteristics of the antenna unit and array meets the engineering requirements in the range of 12 ~ 16 GHz. The maximum gain of the antenna array is 34.3 dBi, and the maximum 3 dB beamwidth is less than 10°. It is confirmed that the designed antenna has the characteristics of high gain, narrow beam, and low profile, and realizes two-dimensional beam scanning in the range of 6 ~ 79° in the elevation plane, which meets the requirements of the Satellite Communications On-the-Move system (SOTM).

1. INTRODUCTION

With the continuous maturation and the deepening research of communication technologies such as cloud computing and big data, traditional communication networks have gradually stepped into the 5G and 6G era. There are explosive growth in the number of users and increasing demand for wide-bandwidth, high-speed, and low-latency communications in this period [1]. To meet the communication needs of massive users and solve real-time communication problems in complex and variable environments, satellite communication systems with their large spatial span, wide coverage, high robustness, strong anti-destruction capability, high-cost performance and diversity of user networks have attracted extensive attention [2, 3]. Satellite Communications On-the-Move system (SOTM), which can solve the problem of real-time motion communication of mobile carriers, has great potential for the communication services such as emergency communication after disasters, real-time communication in war zones, and live broadcasting of sports and cultural activities [4]. Many countries have proposed the plan to build communication networks by using low-orbit satellites to achieve global coverage of mobile communications [5], including the *Starlink program* of the U.S. and the *Hongyun Project* of China. Satellite orbit resources are increasingly depleted, and spectrum resource is getting tighter with the deployment of a large number of high, medium, and low orbit satellites around the world. In order to better use the limited resources to satisfy the needs of SOTM, the SOTM ground station antenna with lightweight, miniaturization, low-profile, high-gain, and beam scanning characteristics has gradually become the development trend of antenna technology [6].

Received 26 September 2022, Accepted 12 November 2022, Scheduled 24 November 2022

* Corresponding author: Shufu Dong (shufudong@163.com), Qiurong Zheng (zqr1620@sina.com).

¹ Information and Navigation College, Air Force Engineering University, Xi'an 710077, China. ² Graduate School, Air Force Engineering University, Xi'an 710077, China. ³ Unit 93110, Air Force, Beijing, China.

The traditional SOTM ground station antennas, which have their advantages and different application scenarios, mainly include parabolic antenna, reflector antenna, phased array antenna, and waveguide slot antenna. The parabolic antennas with high profile are suitable for fixed-station communication such as point-to-point microwave relays; however, it does not apply to mobile carrier communications [7]. Although the reflector antenna has high-gain and wide bandwidth, the weight of the device is too heavy, and the installation is too complicated to apply to small mobile carriers [8]. The phased array antennas, which have a large number of T/R components and phase shifters, not only have the advantages of small size and light weight but also have the advantages of strong anti-interference ability, high scanning rate, and ease of installation. The 1D and 2D scanning can be realized by phase change. However, the high cost and complex construction have resulted in the fact that the phased array antenna is mainly used in the military field and difficult to be applied in the civil field on a large scale [9]. Waveguide slot antenna is widely used in microwave and radar systems owing to its small size, light weight, high aperture efficiency, and narrow main lobe beam, but its design is so complicated that the processing accuracy has a huge impact on antenna performance, which limits the application of waveguide slot antenna, especially at high-frequency bands [10].

Continuous Transverse Stub (CTS) antenna based on parallel plate waveguide (PPW) was first proposed by Hughes Aircraft Company in the 1990s. The antenna adopts the leaky wave antenna theory, which has the advantages of compact structure, high gain, and easy integration. It can realize two-dimensional beam scanning by changing the waveguide frequency or the dielectric constant of the material; nevertheless, its beam scanning angle is severely limited [11–14]. A Variable Inclination Continuous Transverse Stub (VICTS) array antenna is developed on the basis of series-feed CTS antenna, which not only has high gain, low-profile, wide-bandwidth, and beam scanning characteristics, but also can be conformally installed on mobile carriers [15]. The VICTS antenna realizes the beam scanning in the elevation plane by the relative rotation between the radiation layer and feed layer [16]. Precise satellite alignment can be realized by the combination of beam scanning characteristics and a servo control system.

In this paper, we have firstly retrieved and read carefully some of the published VICTS antennas with beam scanning performance, and the structure proposed in these papers have been studied and discussed in depth simultaneously. Then, we proposed a novel VICTS antenna unit and array with linear-gradient stub after a comprehensive analysis and comparison of the antenna structure and performance, described in Table 1. The conventional stepped VICTS antenna stub was optimized to linear-gradient stub in this model. Meanwhile, the matching impedance characteristics and bandwidth of this antenna were further enhanced by adding matching structures on both sides of the stub and a linear slow wave structure at the bottom of the PPW. We also designed a bow-parabolic box antenna and a double-layer transition waveguide structure to feed the prototype antenna. Finally, the antenna element and array are modeled and analyzed by using ANSYS HFSS software, and a microwave anechoic chamber is used to test the antenna prototype. The test data agree well with the simulation results, which means that the model has good electrical parameter performance and beam scanning characteristics. Most importantly, the model is overall light weight and can be conformally mounted on common mobile carriers without additional burden.

Table 1. The structures and performance of the VICTS antenna in different references.

References	Structure	Bandwidth(GHz)	Scanning Features(°)
8	Nonlinear Slow-Wave Structure	13.75~14.5	-5~-70, 5~70
9	Parallel plate with slow-wave corrugation	14.0~14.5	-5~-65, 5~65
17	Two-Types Stubs	13.0~15.0	-6.7~-53, 6.7~53
21	Fed by a Ridged Waveguide Slot	15.32~15.86	-30~30
22	Feeding Network and Slotted Plate	60.0	-60~60

2. FUNDAMENTAL THEORY ANALYSIS

As shown in Fig. 1, the VICTS antenna is mainly composed of two parts: the radiation layer and feed layer. The radiation layer, which is located in the upper part of the PPW, consists of a set of uniformly arranged transverse stub units, and each transverse stub unit is made up of a metal plate with a long straight slot and two matching structures. The feed layer consists of a PPW, an LSG, and linear slow wave structure (SWS). A bow-parabolic box antenna and a double layer transition waveguide structure are used together to feed the proposed antenna array in this paper.

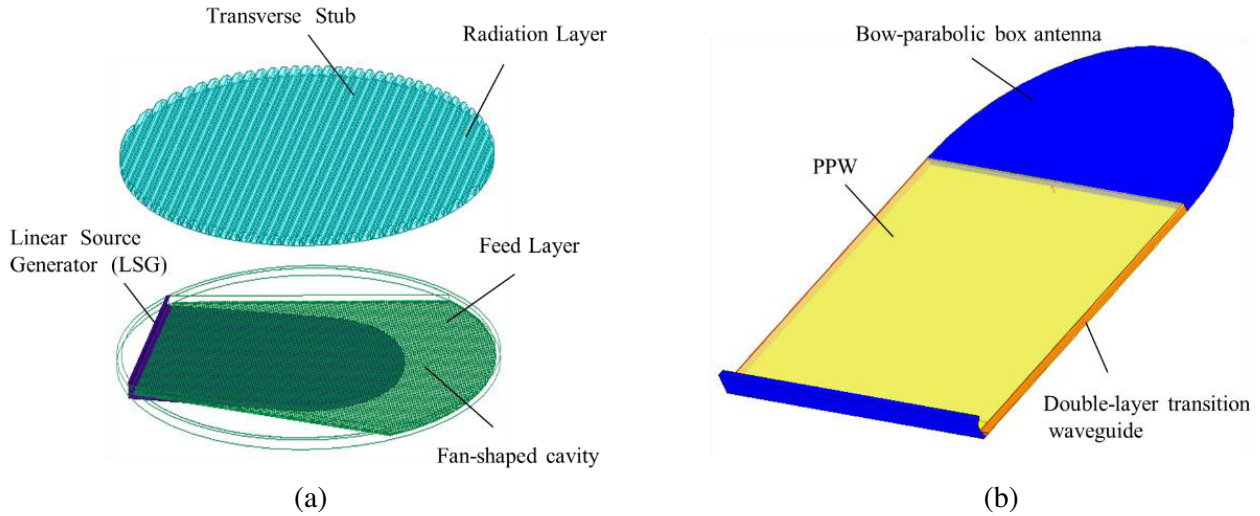


Figure 1. Model diagram of the VICTS antenna. (a) Antenna array, (b) antenna feed structure.

The radiation principle of the VICTS antenna is as follows: the TEM wave or quasi-TEM wave is reflected by the LSG to form a planar wave, which is fed into the input of PPW through the reflection of the double-layer transition waveguide structure. Due to the existence of several long straight slots on the top plate of PPW, resulting in the current on the upper surface, exciting electromagnetic waves radiate into free space through the gap structure of the transverse stub [17, 18].

As shown in Fig. 2, the two-dimensional beam scanning in the elevation plane of the VICTS antenna can be achieved by rotating the radiation layer. Let the incident wave fed into the PPW be horizontal while assuming that the radiation layer rotation angle is α , the length of the radiation stub is l ; the phase at the bottom is φ_0 ; and the phase constant is β , then the phase distribution at the top of the radiation stub is shown in Equation (1).

$$\varphi = \beta l \sin \alpha + \varphi_0, \quad (0 \leq l \leq L) \tag{1}$$

The radiating stubs are subdivided into radiation micro-elements closely aligned with each other by using the idea of differentiation. Assuming that the spacing of individual micro-element is dl , and the phase difference of adjacent micro-elements is $\beta dl \sin \alpha$. According to the radiation theory of phased array antenna, its maximum radiation direction must meet Equation (2) after rotating the antenna radiation stub α angle.

$$\cos \theta_m = \frac{\beta dl \sin \alpha}{\beta dl} = \sin \alpha \tag{2}$$

From Equation (2), it can be seen that the maximum radiation direction of the antenna produces a deviation, which proves that the antenna can change the phase difference between adjacent array elements through the rotation of the radiation layer, thus controlling the radiation direction of the antenna array and realizing two-dimensional beam scanning.

The VICTS antenna is a linearly polarized antenna, where the E -plane, H -plane, and radiation stubs are always perpendicular to each other. Let the antenna elements be arranged in parallel along

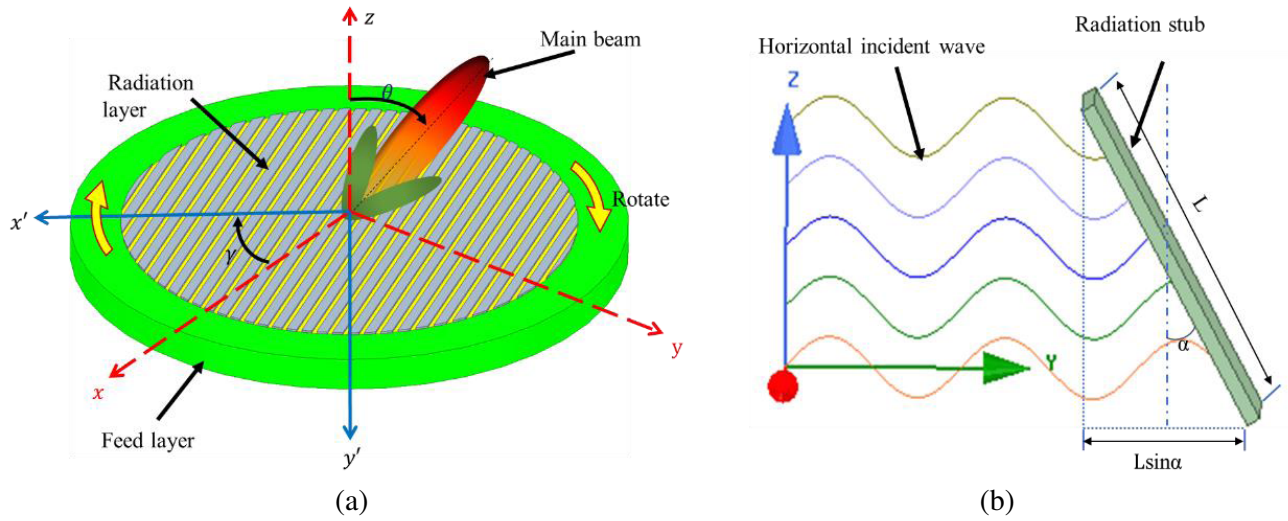


Figure 2. Mechanical scanning diagram of VICTS antenna. (a) Schematic diagram, (b) principle diagram.

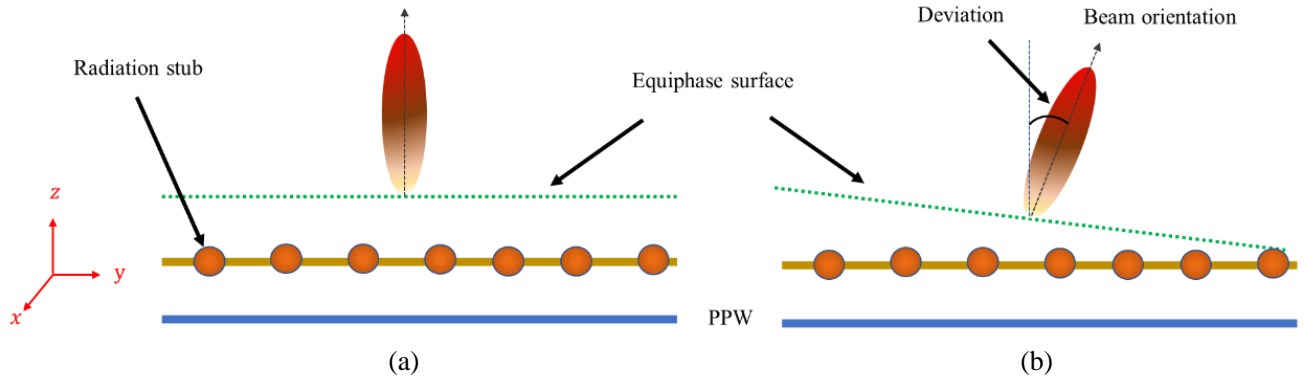


Figure 3. Schematic diagram of VICTS antenna beam scanning. (a) The radiation layer and the feed layer have no relative rotation, (b) the radiation layer and the feed layer produce relative rotation.

the Y -axis, and the space rectangular coordinate system is defined according to the right-handed rule. When the radiation layer and feed layer have not produced relative rotation, the equiphase surface of the antenna is parallel to H -plane, and the main beam points to E -plane, as shown in Fig. 3(a). When the radiation layer and feed layer have produced relative rotation, the equiphase surface of the antenna changes continuously, which will drive the H -plane to continuously change and cause tilting of the beam orientation, as shown in Fig. 3(b). When the rotation angle increases or decreases continuously from 0° , a continuous main beam scanning is achieved in the E -plane. When the rotation angle is equal to 45° , the tilt angle of the main beam is theoretically maximized, but the main beam in the E -plane will still be slightly shifted with the rotation angle due to the interference of the electromagnetic wave distribution in the PPW by the rotation slot [9].

The phase difference of the H -plane is determined by the PPW wavelength when the rotation angle is fixed, so it is necessary to shorten the wavelength of the PPW as much as possible to increase the maximum tilt angle of the main beam. A common method is to fill or partially fill other materials between the PPWs to shorten the wavelength by increasing the dielectric constant, whereas this method will not only increase the weight and transmission loss of the antenna but also reduce the antenna gain. In this paper, we adopt periodic SWSs of equal height at the bottom of PPW to increase the equivalent dielectric constant and shorten the wavelength of PPW. This method not only reduces the transmission

loss but also avoids the end-emission phenomenon. The equivalent permittivity ϵ_e of the antenna element after using this structure can be calculated by Equation (3), where β_{-1} is the propagation constant of the first harmonic, β_0 the free-space propagation constant, and d the center distance of the adjacent antenna element [19].

$$\epsilon_e = \left(\frac{\beta_{-1} + 2\pi/d}{\beta_0} \right)^2 \tag{3}$$

3. DESIGN AND DISCUSSION

3.1. Model Design of the Unit and Array

The closed expression of the VICTS antenna is derived in [20], but this expression is too complex to be applied in engineering practice. This paper ignores the transmission loss and other secondary factors in the design of the antenna element, and the radiation stub is regarded approximately equivalent as a T-shaped interface, hence the proportion relation (see Equation (4)) in the Reference [19] is used as the design principle of the VICTS antenna element.

$$|K^2| \propto \frac{\omega}{2h} \tag{4}$$

According to Equation (4), the ratio of stub width ω and PPW height h is directly proportional to the radiation coupling coefficient $|K^2|$. h is generally fixed in engineering practice to further simplify the actual operation, and the radiation energy is controlled by changing ω . With the gradual increase of radiated energy, ω will become larger and larger, which leads to the gradual deterioration of the reflection coefficient and makes the overall performance of the array model degrade sharply. To alleviate the degradation speed of array performance, the matching structure is introduced into both sides of the stub to reduce the reflection coefficient of the antenna array effectively. The comparison of simulation results before and after adding the matching structure to the cells is shown in Fig. 4. It can be found that the electric and magnetic fields on both sides of the stub are strengthened with the addition of the matching structure, and the distribution is more concentrated and more directional. However, the matching element will affect the port phase, which needs to be considered comprehensively in array design.

When the center distance d of adjacent elements is equal to the wavelength of the plane wave, the superposition of reflected waves generated by each element will deteriorate the port characteristics

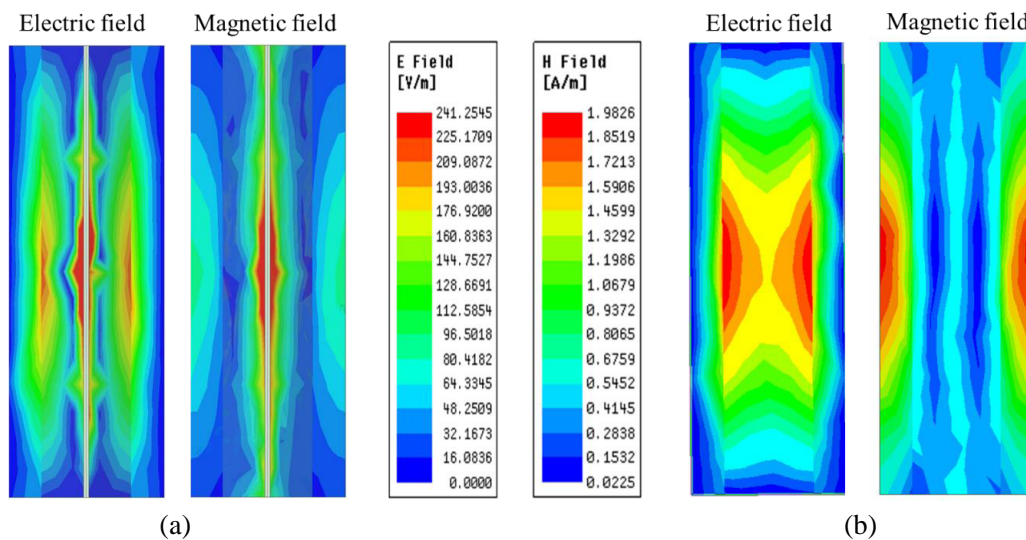


Figure 4. Comparison diagram of EM field distribution of the VICTS antenna. (a) No matching structure is added to the cell, (b) add matching structure to the cell.

of the array antenna, resulting in the phenomenon of grating lobes. The phenomenon will not only increase the radiation loss, but also disperse the radiation energy and reduce the effective radiation ultimately. Therefore, the maximum value range of d is usually determined by Equation (5) to suppress the appearance of grating lobes in array design.

$$d \leq \frac{\lambda}{1 + \sin \theta_m} \quad (5)$$

where λ is the free-space electromagnetic wave wavelength, and θ_m is the maximum tilt angle of the main beam. For the convenience of modeling and engineering applications, d is usually taken to be slightly smaller than the plane wave wavelength, but this way of taking values will lead to a slight deviation of the main beam in the elevation plane direction.

According to the above theory and principles, this paper constructed the VICTS antenna cell and array model with linear gradient stubs working at 12–16 GHz. The antenna unit model is shown in Fig. 5(a), and its main parameters after optimization are shown in Table 2. A circular array with a radius of 300 mm is composed of a series of antenna units of suitable length placed in parallel along the Y axis, and its top view and main view are shown in Fig. 5(b) and Fig. 5(c), respectively. Compared with the traditional VICTS antenna, the introduction of a linear gradient structure and matching structures achieves wider impedance matching characteristics and increases the antenna bandwidth. Meanwhile, the periodic SWSs of equal height shorten the PPW wavelength, reduce the transmission loss, and improve the antenna gain.

To improve the directionality of beam transmission energy and reduce energy leakage or collapse, metal plates are used to encapsulate both sides of the feed port, as shown in the green edge of Fig. 1. The PPW, metal plate, feeding port, and antenna outer wall form a fan-shaped cavity, and then this

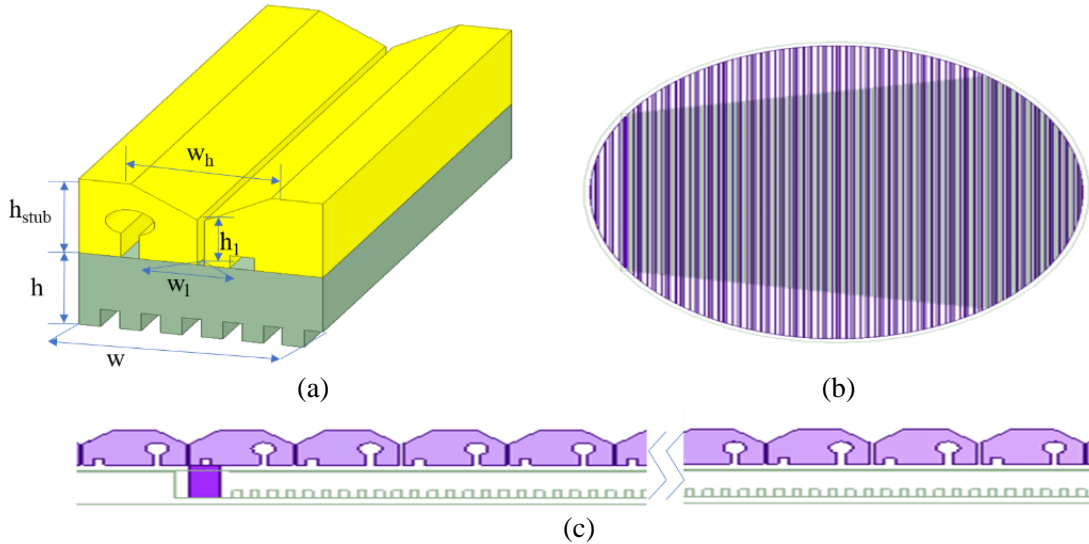


Figure 5. Model diagram of the VICTS antenna unit and array. (a) Model diagram of the antenna unit, (b) the top view of the antenna array, (c) the main view of the antenna array.

Table 2. Main parameters of VICTS antenna unit (mm).

w	h	h_1	w_1	h_{stub}	w_h
17.29	9.9	6.2	0.54	10.2	9.93

cavity, radiation layer, and feeding layer form a quasi-parallel plate transmission line structure together, thus, plane waves can radiate from transverse stub to free space in the process of transmission.

3.2. Feed Design of Array Antenna

The main transmission structure of the VICTS antenna is PPW, and its structural characteristics need to be fed by a linear feed source. Common linear feed sources include discrete line sources such as slot-array antennas of rectangular waveguides and continuous line sources, for instance, the H -plane horn antennas and parabolic antennas. Among them, the discrete line source processing is more difficult, and the tensor angle of the H -plane horn antenna feed source will affect the aperture surface phase. If the phase difference is too large, it easily leads to the distortion of the pattern, resulting in a significant drop in gain. Array antennas arranged in a straight line are often fed in parallel and series. In addition, VICTS array antennas need to be rotated to achieve beam scanning, and it is inconvenient to rotate when using the parallel feed. Taking the above factors into consideration, this paper selects a bow-parabolic box antenna as the LSG and uses a double-layer transition waveguide structure to realize the propagation of plane waves. As seen in Fig. 6(a), both of them form the antenna feed structure together.

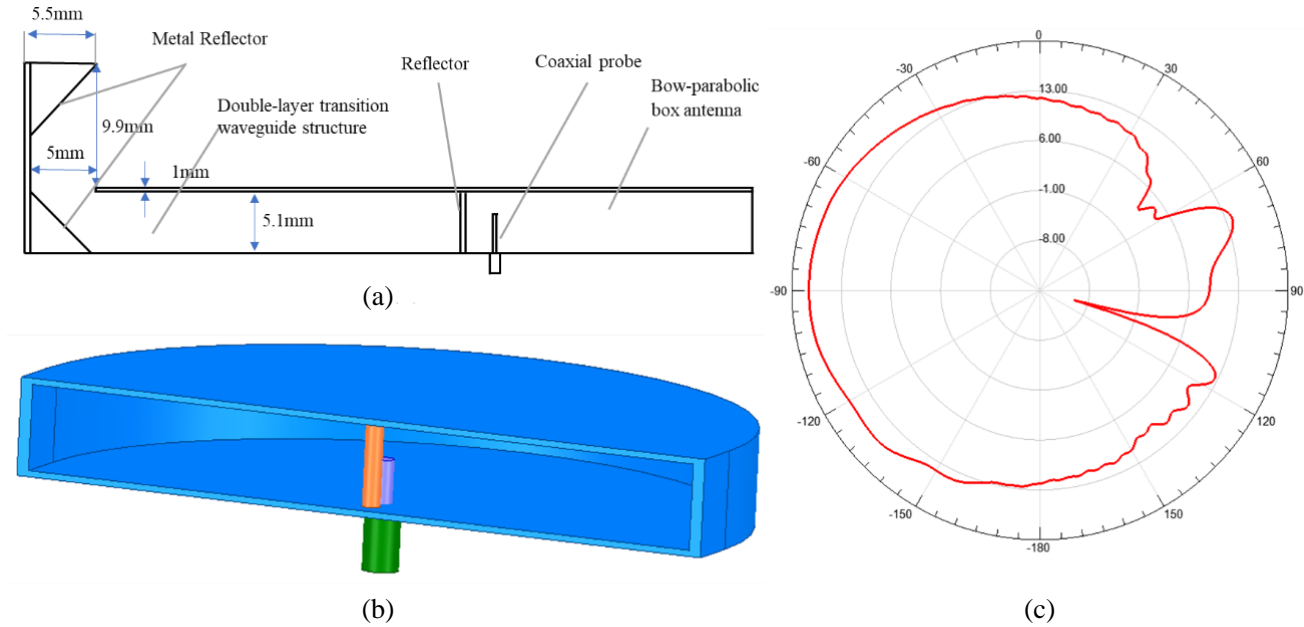


Figure 6. Diagram of the antenna feed structure. (a) The main view of the feed structure, (b) model diagram of LSG, (c) H -plane directional diagram of LSG.

The model diagram of the bow-parabolic box antenna is shown in Fig. 6(b). Its main body consists of a parabolic box antenna, which is constructed of pec material. The coaxial probe is placed at the focal point of the parabolic box, and the reflector is placed at $1/4$ wavelength behind the coaxial probe to ensure that the feed source radiates toward the parabolic direction. The material copper is used for the coaxial probe and reflector. Due to the geometrical characteristics of the paraboloid, the electromagnetic waves of TEM mode or quasi-TEM mode emitted from the focal point are reflected by the paraboloid to form mutually parallel plane waves. ANSYS HFSS software was used to model and simulate the above feed source, and its directional diagram of the H -plane is shown in Fig. 6(c), showing that the feed source has good directionality from the results.

The double-layer transition waveguide is mainly composed of the PPW structure, including the array antenna and parabolic box antenna's PPW structure, respectively. This structure is designed to transfer the plane wave beam to the PPW input port of the VICTS array antenna, which is achieved

by two metal reflector plates placed at 45° . To avoid the dissipation of radiated energy, the structure needs to be encapsulated with metal materials, except for a 5.0 mm long slot at the left end of the metal plate connecting the upper and lower layers.

4. EXPERIMENT AND COMPARISON

To verify the feasibility of the design scheme, the VICTS antenna unit and array proposed above were modeled and simulated by ANSYS HFSS software according to the parameters in Table 2. At the same time, a manufacturing antenna with a 300 mm radius was made by numerical control processing technology and measured in a microwave anechoic chamber. The manufacturing antenna and test environment are shown in Fig. 7. The results show that the reflection coefficient of the array antenna measured by Agilent N5230A and the S_{11} parameter of the array model calculated by simulation software are both less than -10 dB in the operating frequency range of 12–16 GHz (as shown in Fig. 8), which proves that the model can meet the needs of engineering applications.

The 3D far-field radiation patterns of the antenna elements at different frequencies are shown in Fig. 9. The data shows that the element radiation pattern has almost no relationship with the frequency point selection. The radiation energy is mainly distributed in a circular shape, with small portions of end-emission and leakage energy on both sides and the bottom of the stub. Although the shape of the



Figure 7. Diagram of the manufacturing antenna and test environment.

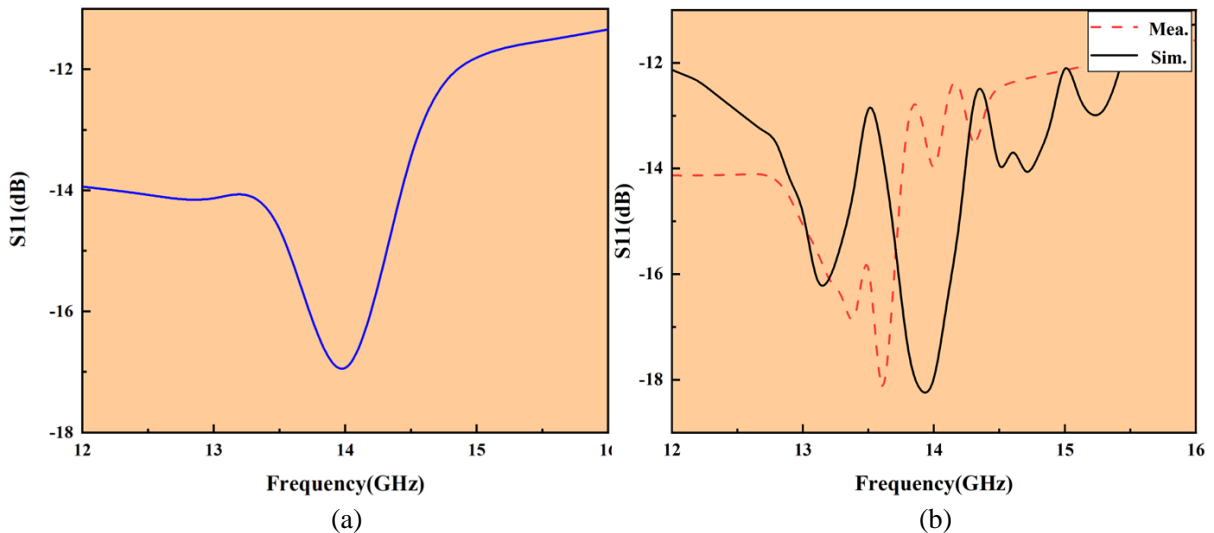


Figure 8. Reflection coefficients of the VICTS antenna. (a) Antenna unit, (b) antenna array.

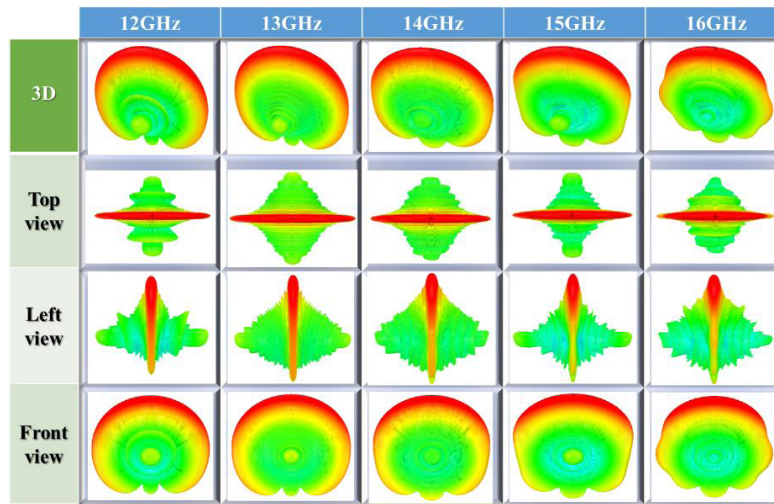


Figure 9. The 3D far-field radiation patterns of the VICTS antenna elements at different frequencies.

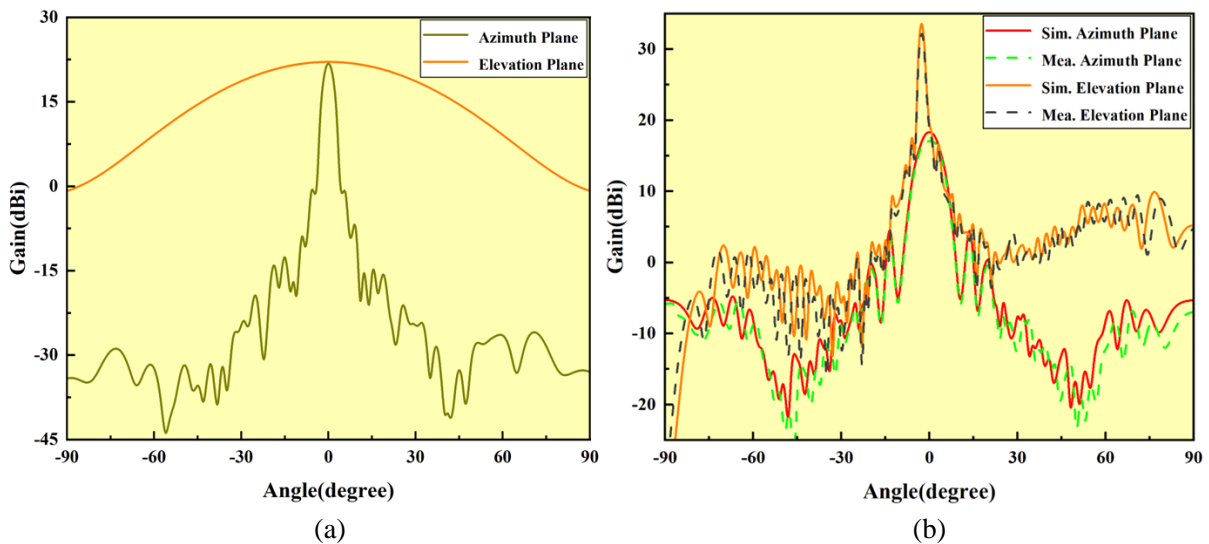


Figure 10. The radiation pattern of the VICTS antenna at 14.5 GHz. (a) Antenna unit, (b) antenna array.

energy distribution is slightly distorted when the frequency point tends towards high frequencies, the radiation direction is hardly affected, which proves that the antenna element has good directionality in the frequency range of 12–16 GHz.

The radiation pattern of the antenna unit in elevation planes and azimuth planes at 14.5 GHz is shown in Fig. 10(a), showing that the maximum gain of the antenna element is 22.6 dBi, and the sidelobes level is low. Fig. 10(b) shows the radiation patterns of the manufacturing antenna and the simulated antenna in the elevation plane and azimuth plane at 14.5 GHz. The data of measured and simulated diagrams are in good agreement. Both of them not only have a narrow main lobe beamwidth but also have concentrated energy and good directionality. However, the sidelobe level increases significantly due to the mutual coupling and interaction between the individual units. At 14.5 GHz, the maximum gain in the elevation plane is 34.3 dBi in the simulated data, and the measured gain is about 1 dBi lower than the simulated data. The possible reason for this phenomenon may be insufficient processing accuracy and poor metal encapsulation, but this does not have a significant impact on the beam scanning performance

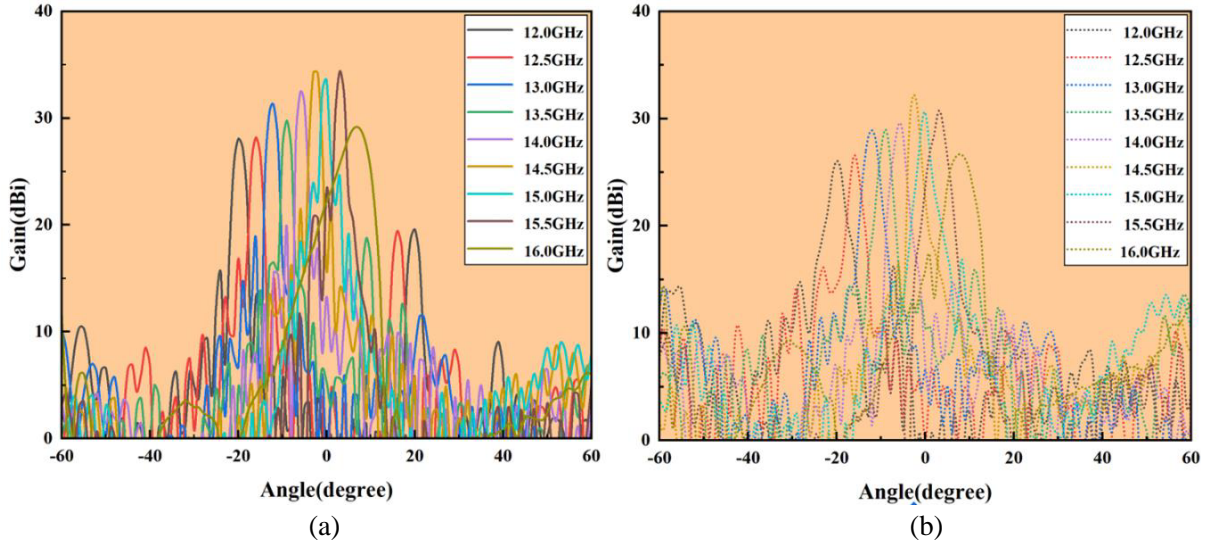


Figure 11. The radiation pattern of the VICTS antenna array at different frequencies. (a) Simulation pattern, (b) measured pattern.

of the antenna. It can be seen from the data that the beam orientations of the two patterns are almost the same.

When there is no relative rotation between the radiation layer and feed layer, the radiation diagram of the array antenna at different frequencies in the elevation plane is shown in Fig. 11, from which it can be seen that the measured and simulated results of the antenna have nearly the same beam direction. It implies that the designed antenna has obvious frequency scanning characteristics, which can work by changing the antenna of the center frequency to realize elevation plane beam scanning on a small scale. At the frequency range of 12–16 GHz, this array antenna has a beam sweep range of -21° to 7° in the elevation plane with no more than a 7 dBi decrease in antenna gain. Fig. 11 also shows that the main beam will still be offset in the vertical direction even if the radiation and feed layers are not rotated, and the offset angle is roughly consistent with the elevation angle calculated by the uniform linear array theory, which is caused by the fact that VICTS antenna is a traveling wave antenna.

Figures 12 and 15 also show that the beam scanning angle increases with the increase of the rotation angle, and there is a nonlinear correspondence between the two. At the same time, the 3 dB beamwidth of the VICTS antenna is still narrower overall, although it also increases. When the rotation angle is $0 \sim 40^\circ$, the scanning angle is correspondingly $6 \sim 54^\circ$, and the 3 dB beamwidth is kept within 7° . If the servo control system can be combined, the rotation angle can be increased to 50° , and the corresponding scanning angle can be increased to 79° with a 3 dB beamwidth that does not exceed 10° at this case. When the radiating and feed layers are rotated clockwise, it is easy to obtain the scanning range of $-6 \sim -79^\circ$ for the elevation angle due to the symmetry of the circular antenna.

The normalized SLL of this antenna is shown in Table 3 with different rotation angles at 14.5 GHz. The VICTS antenna can be equated to discrete point source array. The distance between the discrete point sources is minimum when the rotation angle $\gamma = 0^\circ$, and the antenna gain is maximum. The spacing between discrete point sources has increased with the continuous increase of rotation angle and resulted in the antenna main-lobe beam tilt. This phenomenon caused the main-lobe gain to decrease and the sidelobe level to increase significantly, which can be clearly seen in Table 3. Although the rotation angle can be barely increased to more than 45 degrees by increasing the dielectric constant with various methods, the antenna main lobe gain decreases significantly, and the SLL rises significantly. In this case, it is necessary to combine the servo control system with high precision and make decisions based on the predicted spatial position to realize the beam scanning function.

The polarization pattern of the VICTS antenna array is shown in Fig. 13 and Fig. 14. As can be seen in Fig. 13, the antenna has great polarization isolation and outstanding cross-polarization characteristics at different frequencies when $\gamma = 0^\circ$. With the gradual increase in the rotation angle, the polarization

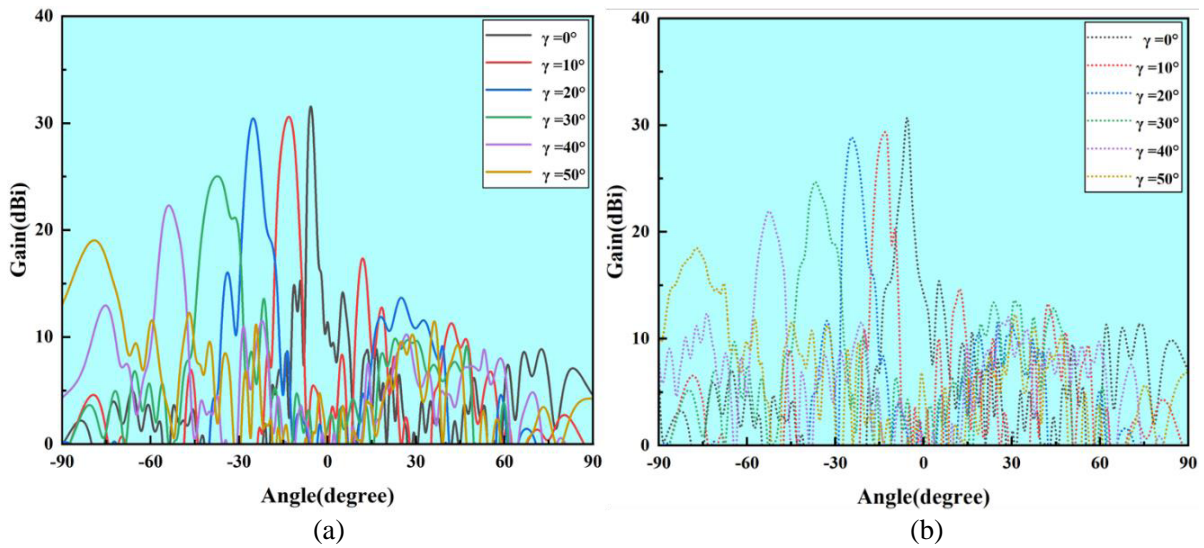


Figure 12. The radiation pattern of the VICTS antenna array at different rotation angles at 14.5 GHz. (a) Simulation diagram, (b) measured diagram.

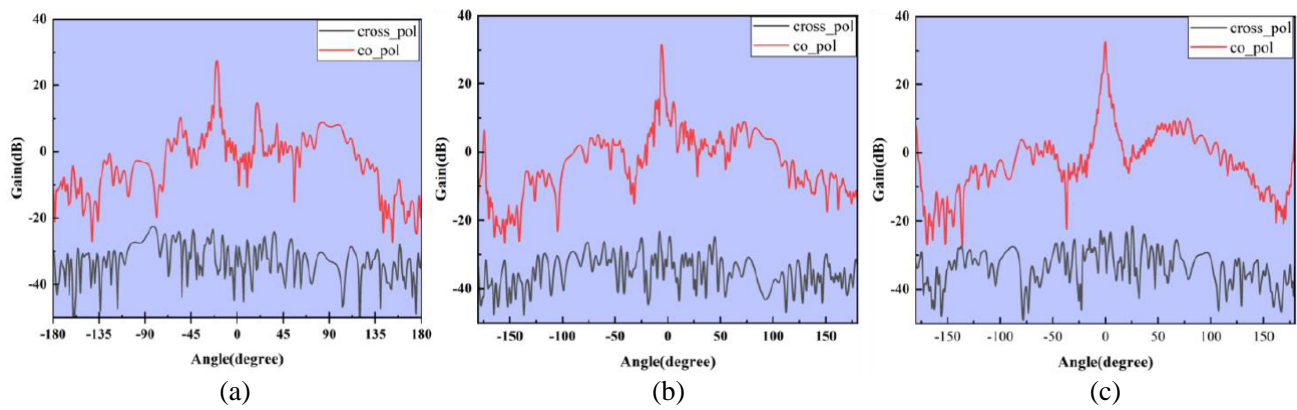


Figure 13. Polarization pattern of the VICTS antenna array at different frequencies. (a) 13 GHz, (b) 14 GHz, (c) 15 GHz.

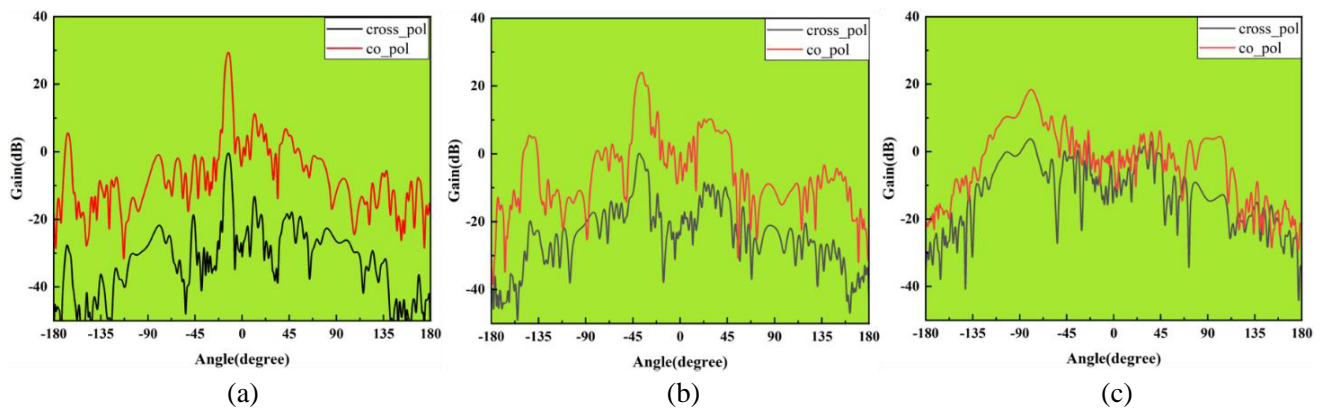


Figure 14. Polarization pattern of the VICTS antenna array with different rotation angles at 14.0 GHz. (a) $\gamma = 10^\circ$, (b) $\gamma = 30^\circ$, (c) $\gamma = 50^\circ$.

Table 3. The normalized SLL of the VICTS antenna with different rotation angles.

Rotation Angles(°)	0	10	20	30	40	50
Simulation of Normalized SLL (dB)	-19.8	-18.8	-18.3	-14.1	-12.6	-9.4
Measurement of Normalized SLL (dB)	-18.6	-17.2	-16.6	-12.9	-10.7	-7.3

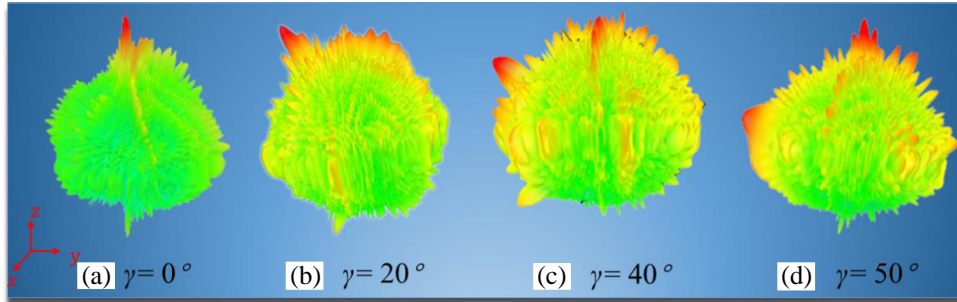


Figure 15. The 3D far-field radiation pattern of the VICTS antenna array at different rotation angles.

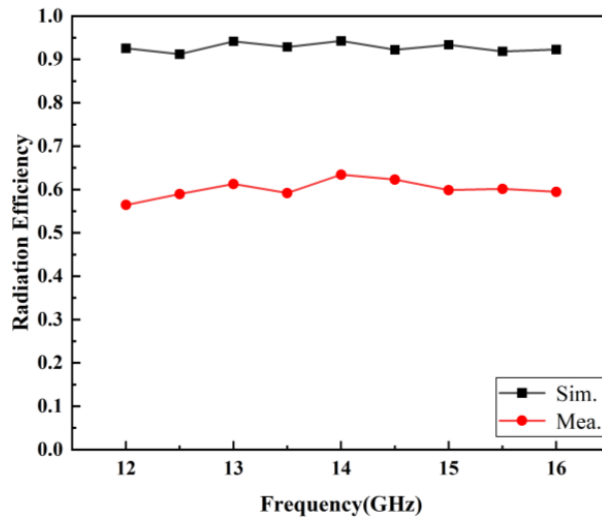


Figure 16. The radiation efficiency pattern of the VICTS antenna array.

isolation tends to decrease, which is shown in Fig. 14. The rise of the interference from co-polarization and cross-polarization leads to the deterioration of antenna gain with increasing rotation angle.

The radiation efficiencies of this antenna at different frequencies are shown in Fig. 16, which can be obtained by the ratio of peak realized gain and peak directivity in ANSYS HFSS software, and the measured radiation efficiency can also be achieved by comparing the accepted power of the receiving horn antenna with the input power of this antenna. It can be seen from the data that there is a large gap between the simulated radiation efficiency and measured radiation efficiency. The reason that this antenna radiation efficiency can reach about 93% is that the software provides an ideal simulation environment, and not considers transmission loss, feed loss, packaging, and other factors. However, these losses cannot be ignored in the actual measurement. Coupled with the impact of the antenna processing accuracy, poor packaging, and other factors, the measured radiation efficiency of this antenna can only reach about 60%.

Other works have carried out extensive exploration and research on the application of VICTS antennas and designed a variety of different types of VICTS antennas in recent years [21, 22]. A comparison of the antenna designed in this paper with the published CTS antennas and VICTS antenna is shown in Table 4, where the data show that this new antenna has an improved scanning range.

Table 4. Comparison of antenna performance in different references.

References	Bandwidth(GHz)	Scanning Features(°)	Maximum Gain(dB)	SLL(dB)	Radiation Efficiency
8	13.75~14.5	-5~70, 5~70	30	-18	Not Given
9	14.0~14.5	-5~65, 5~65	Approximately 32	Not Given	Not Given
17	13.0~15.0	-6.7~53, 6.7~53	Approximately 30	-19	Not Given
21	15.32~15.86	-30~30	Approximately 30	-25	60%
22	60.0	-60~60	29.3	-15	62%
This Paper	12.0~16.0	-6~79, 6~79	34.3	-18.1	Approximately 60%

5. CONCLUSION

In summary, the VICTS unit and array with linear-gradient stub are modeled and simulated in ANSYS HFSS software. A bow-parabolic box antenna and a double-layer waveguide structure are used as the antenna feed source, while an antenna prototype is fabricated and tested. The full-wave simulation and test results confirm that the proposed antenna model not only has the characteristics of high gain, narrow beam, and low profile but also can achieve beam scanning in the range of $6 \sim 79^\circ$ and $-6 \sim -79^\circ$ in the elevation plane. Compared to conventional VICTS antennas, the beam scanning performance has been improved to better meet the requirements of SOTM. Further research is needed to investigate ways to increase the rotation angle while maintaining the main lobe gain or reducing the sidelobe level to achieve a larger angle beam scanning.

REFERENCES

1. Aguado-Agelet, F., A. E. Villa, M. Arias-Acuna, and F. J. Diaz-Otero, "AOCS requirements and practical limitations for high-speed communications on small satellites," *International Journal of Aerospace Engineering*, Vol. 2019, 1–16, 2019.
2. Ssimbwa, J., B. Lim, J.-H. Lee, and Y.-C. Ko, "A survey on robust modulation requirements for the next generation personal satellite communications," *Frontiers in Communications and Networks*, Vol. 3, 2022.
3. Liu, T., C. H. Sun, and Y. S. Zhang, "Load balancing routing algorithm of low-orbit communication satellite network traffic based on machine learning," *Wireless Communications & Mobile Computing*, Vol. 2021, 2021.
4. Yuan, D., Y. Y. Qin, Z. W. Wu, and X. W. Shen, "An emergency positioning system fusing GEO satellite doppler observation and INS for SOTM," *IEEE Transactions on Instrumentation and Measurement*, Vol. 70, 2021.
5. Pearson, R. A., J. Vázquez, and M. W. Shelley, "Next generation mobile SATCOM terminal antennas for a transformed world," *European Conference on Antennas and Propagation*, 2341–2345, 2011.
6. Torabi, Y., G. Dadashzadeh, A. Lalbakhsh, and H. Oraizi, "High-gain and low-profile dielectric-image-line leaky-wave-antenna for wide-angle beam scanning at sub-THz frequencies," *Optics and Laser Technology*, Vol. 150, 2022.

7. Johnson R. C. and H. Jasik, *Antenna Engineering Handbook*, McGraw-Hill Book Company, New York, 1984.
8. Wang, K., X. Lei, J. Gao, T. Li, S. Tian, and M. Zhao, "A low-sidelobe-level variable inclination continuous transverse stub antenna with a nonlinear slow-wave structure," *International Journal of Antennas and Propagation*, Vol. 2021, 1–10, 2021.
9. Wei, M., J. Liu, H. X. Li, and S. Y. Liu, "Design of a variable inclination continuous transverse stub array," *12th International Symposium on Antennas, Propagation and Electromagnetic Theory (ISAPE)*, Hangzhou, 2018.
10. Yan, L., W. Hong, G. Hua, J. X. Chen, K. Wu, and T. J. Cui, "Simulation and experiment on SIW slot array antennas," *IEEE Microwave and Wireless Components Letters*, Vol. 14, No. 9, 446–448, 2004.
11. Henderson, W. H. and W. W. Milroy, "Wireless communication applications of the continuous transverse stub (CTS) array at microwave and millimeter wave frequencies," *IEEE/ACES International Conference on Wireless Communications and Applied Computational Electromagnetics*, 253–256, Honolulu, 2005.
12. Kim, W., M. F. Iskander, and W. D. Palmer, "An integrated phased array antenna design using ferroelectric materials and the continuous transverse stub technology," *IEEE Transactions on Antennas and Propagation*, Vol. 54, No. 11, 3095–3105, 2006.
13. Milroy, W. W., S. B. Coppedge, and A. C. Lemons, "Variable inclination continuous transverse stub array," *US Patent*, 6919854B2, 2005.
14. Milroy, W. W., "The continuous transverse stub (CTS) array: Basic theory, experiment, and application," *Proceedings of the Antenna Applications Symposium*, 252–283, 2005.
15. Hao, R. S., Y. J. Cheng, and Y. F. Wu, "Shared-aperture variable inclination continuous transverse stub antenna working at K- and Ka-bands for mobile satellite communication," *IEEE Transactions on Antennas and Propagation*, Vol. 68, No. 9, 6656–6666, 2020.
16. Gao, J., X. Lei, J. Wu, and T. Li, "Theoretical model for patterns of VICTS antenna," *IEEE 17th International Conference on Communication Technology (ICCT)*, 728–731, Chengdu, China, 2017.
17. Wang, K., X. Lei, J. Gao, T. Li, and M. Zhao, "A low-sidelobe-level variable inclination continuous transverse stub antenna with two-types stubs," *2021 IEEE 4th Advanced Information Management, Communicates, Electronic and Automation Control Conference (IMCEC)*, Chongqing, China, 2021.
18. Wang, K., X. Lei, J. Gao, T. P. Li, and M. Y. Zhao, "A low-sidelobe-level variable inclination continuous transverse stub antenna with two-types stubs," *2021 IEEE 4th Advanced Information Management, Communicates, Electronic and Automation Control Conference (IMCEC)*, Vol. 4, 1554–1558, 2021.
19. Gao, J., X. Lei, G. H. Chen, Y. Zhang, and J. M. Wu, "Design of the variable inclination continuous transverse stub antenna based on rectangular grating slow-wave structure," *International Journal of Antennas and Propagation*, Vol. 2018, No. 1, ID5793535, 2018.
20. Porter, B. G., "Closed form expression for antenna patterns of the variable inclination continuous transverse stub," *IEEE International Symposium on PAST*, 164–169, 2010.
21. Lu, X., S. Gu, X. Wang, H. Liu, and W. Lu, "Beam-scanning continuous transverse stub antenna fed by a ridged waveguide slot array," *IEEE Antennas and Wireless Propagation Letters*, Vol. 16, 1675–1678, 2017.
22. Karim, T., H. Jiro, S. Ronan, and A. Makoto, "Wideband and large coverage continuous beam steering antenna in the 60-GHz band," *IEEE Transactions on Antennas and Propagation*, Vol. 65, No. 9, 4418–4426, 2017.